Hindawi
Mathematical Problems in Engineering
Volume 2019, Article ID 4329830, 11 pages
https://doi.org/10.1155/2019/4329830

Research Article

Estimation of Rail Axial Force in High-Speed Railway Ballastless Track Based on Wave Modes

Qiang Yi,[1,2] **Cai-you Zhao**,[1,2] **Ping Wang**,[1,2] **Xin Gao**,[1,2] **Liu-cong Wang**,[1,2] **and Wen-hua Ke**[1,2]

[1]*Key Laboratory of High-Speed Railway Engineering, Ministry of Education, Southwest Jiaotong University, Chengdu 610031, China*
[2]*School of Civil Engineering, Southwest Jiaotong University, Chengdu 610031, China*

Correspondence should be addressed to Cai-you Zhao; yqzjswjtu2016@163.com

Received 9 April 2019; Revised 1 June 2019; Accepted 12 June 2019; Published 17 July 2019

Academic Editor: Arkadiusz Zak

To estimate the rail axial force of high-speed railway ballastless track, the reasonable index without complex measuring or error correction process is proposed. Taking the ballastless track structure in high-speed railway as the research object, the wave motion of periodic ballastless track is studied using the wave finite element method. It is found that some standing wave modes are linearly correlated with the rail axial force and thus can be considered as the basic indices for rail axial force estimation. A further in situ experiment according to the modal test method is performed and the feasibility of different wave modes for estimating rail axial force is discussed. Experiment results show that the lateral wave mode coincides well with the theoretical result while there is a large difference for the vertical wave mode. To explicate the difference, the temperature-dependent properties of the fastening are tested additionally. Parametric analysis shows that the frequency shift of vertical wave mode is greatly affected by the fastening temperature-dependent characteristics including the rail pad, elastic pad, and fastener clamping force, while the frequency shift of lateral wave mode is mainly determined by the rail axial force.

1. Introduction

Continuous welded rail (CWR) has been widely applied in high-speed railway lines; however, excessive stress in the rail can be generated with large temperature variation, causing rail buckling or breaking. The axial force of CWR is always a key issue for railway administration department, and the rail axial force estimation methods have also become the focus of researchers.

Methods for estimating rail axial force can be divided into the strain method, stress method, and energy method according to the testing principle. The main techniques of strain method include the resistance strain method [1] and the optical fiber strain method [2, 3], while it is complicated to attach the sensors used in the resistance strain approach and zero drift is unavoidable, and optical fiber strain sensors are expensive and liable to be damaged. The principle of stress method is based on physical changes such as sound, electricity, or magnetism under the stress field of a material including the magnetic method [4], ultrasonic method [5], and X-ray method [6]. The magnetic and X-ray approach can only be adopted to test the surface temperature stress of rail. While for the ultrasonic approach, the testing precision and signal treatment requirements are strict because rail temperature stresses are less sensitive to the acoustic velocity. As for the energy method, dynamic characteristics of CWR can be changed with different internal stresses, and the rail axial force can be evaluated based on the relations between the corresponding dynamic characteristics and stress. The energy methods mainly include the enforced lateral displacement technique [7], rail lifting method [8], and vibration frequency technique [9]. Large machines are needed for the enforced lateral displacement technique and rail lifting approach, affecting the normal operation of railway. Moreover, measurement results might be greatly affected by constraint conditions and boundary conditions for the vibration frequency approach. Therefore, the existing rail axial force estimation methods still have some limitations, such as complicated testing processes, high-precision requirement, or high-cost, and further studies on the rail axial force estimation should be carried out.

Vibration characteristics of rail are closely related to the axial force. Luo [11, 12] established a finite element model for analyzing the response of CWR under axial load and discussed the relations between axial force and rail vibration characteristics. The studies show that the resonance frequency increases while the amplitude decreases nonlinearly with the increase of the rail tension force. In addition, the flexural wavelength of rail changes with the axial force. Damljanović et al. [13] and Kjell et al. [14] evaluated the rail axial force by measuring the flexural wavelength of rail under a fixed excitation frequency by laser vibrometer and accelerometers. However, in this method, some fastenings must be removed, and high precision is also required. Guo et al. [15] analyzed the influence of rail axial force on the dynamic response of vehicle and track. The calculation results show that the dynamic system tends to concentrate the energy towards lower frequency vibration under the effect of rail axial compression force.

To measure the rail axial force in an actual track structure, Aikawa et al. [16] studied the resonance frequencies of ballast track, presenting that the pinned-pinned frequency could be used as the index for measuring rail axial force in ballast track. However, the sensitivity of the experimental result is higher than the numerical one. Since the rail vibration has a close relation with the constraints and boundary conditions, there are numbers of uncertain factors in ballast track structure, such as uncertain fastening stiffness, sleeper spacing, and foundation condition. The rail axial force estimation in ballast track structure will be affected by the uncertain constraints and boundary conditions, and obvious errors might be caused. In order to improve the accuracy for estimating the rail axial force based on the resonance frequency, Urakawa et al. [17] used the receptance function of the rail to evaluate the rail axial force and proposed an error correction method considering the sleeper bays and the wear of the rail head. However, there are still some differences between the experimental results and theoretical results. Besides, it is difficult to conduct the error correction procedure, because the detailed information of the ballast track within 30m is required according to Urakawa's study.

Comparing with ballast track, uncertain factors in ballastless track of high-speed railways are greatly reduced due to the higher requirements of design and construction. Besides, the elasticity of high-speed railway ballastless track structure is mainly provided by the fastenings, and the fastening stiffness of ballastless track is much lower than that of ballast track; thus, the influences from the substructure are weakened. Furthermore, the concrete slab is used in the ballastless track instead of ballast bed; the uncertain constraints and boundary conditions in the ballastless track are further reduced. Therefore, the ballastless track structure in high-speed railway can be considered as an infinite periodic structure [18]. The above characteristics provide more feasibility to estimate the rail axial force accurately in high-speed railway ballastless track by using the vibration technique. This paper presents the theoretical and experimental study on the relative rail axial force estimation in periodic ballastless track structure based on the wave modes. The relations between the relative rail axial force and standing wave modes are discussed. In the estimation method, only a force hammer and a few acceleration sensors are needed for estimating the rail axial force efficiently, and the correction process is not required anymore.

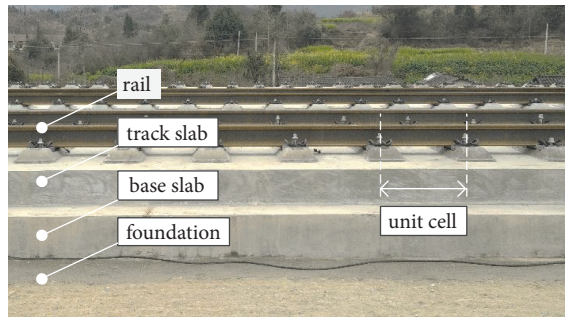

Figure 1: High-speed railway ballastless track.

The outline of the paper is as follows. In Section 2, taking the ballastless track structure in high-speed railway as the research object, infinite periodic track structure models are established considering the rail axial force based on the wave finite element method. An in situ experiment for selecting the reasonable index of rail axial force estimation is performed in Section 3, and the influences of the fastening temperature-dependent parameters are discussed in Section 4. Finally, the paper is concluded in Section 5.

2. Theoretical Study

The ballastless track can be considered as a periodic structure and the wave motion in the rail is mainly determined by the rail itself and the fastening system [19]. Therefore, the rail axial force can be estimated using the rail-fastening model. Since the rail foot is constrained by the fastening and the cross section of the rail is asymmetrical, a simple beam model is not sufficient to describe the wave motion [10, 20, 21]. Therefore, the wave finite element model for the infinite periodic ballastless track structure is established considering the axial force of rail. The dispersion curves and wave modes of the periodic track structure are obtained based on Bloch theorem, and the relations between the wave modes and rail axial force are analyzed accordingly.

Since the ballastless track structure can be considered as an infinite periodic structure, as shown in Figure 1, the wave motions can be obtained within a unit cell using the wave finite element method [22]. The equation of motion for the unit cell is given by

$$\left(\mathbf{K} + \mathrm{i}\omega\mathbf{C} - \omega^2\mathbf{M}\right)\mathbf{U} = \mathbf{F} \tag{1}$$

where ω is the angular frequency, $\mathbf{K}$ is the stiffness matrix, $\mathbf{C}$ is the damping matrix, $\mathbf{M}$ is the mass matrix, and $\mathbf{U}$ and $\mathbf{F}$ are node displacement and force. Equation (1) can be written as follows:

$$\begin{bmatrix} \mathbf{D}_{\mathrm{LL}} & \mathbf{D}_{\mathrm{LI}} & \mathbf{D}_{\mathrm{LR}} \\ \mathbf{D}_{\mathrm{IL}} & \mathbf{D}_{\mathrm{II}} & \mathbf{D}_{\mathrm{IR}} \\ \mathbf{D}_{\mathrm{RL}} & \mathbf{D}_{\mathrm{RI}} & \mathbf{D}_{\mathrm{RR}} \end{bmatrix} \begin{Bmatrix} \mathbf{U}_{\mathrm{L}} \\ \mathbf{U}_{\mathrm{I}} \\ \mathbf{U}_{\mathrm{R}} \end{Bmatrix} = \begin{Bmatrix} \mathbf{F}_{\mathrm{L}} \\ \mathbf{F}_{\mathrm{I}} \\ \mathbf{F}_{\mathrm{R}} \end{Bmatrix} \tag{2}$$

Table 1: Track structure parameters.

Elastic modulus of rail E (Pa)	Density of rail ρ (kg/m^3)	Sectional area of rail A (cm^2)	Sectional inertia moment of rail I_z (m^4)
2.06e11	7850	77.45	524e-8
Sectional inertia moment of rail I_y (m^4)	Vertical stiffness of fastening k_z (kN/mm)	Lateral stiffness of fastening k_y (kN/mm)	Longitudinal stiffness of fastening k_x (kN/mm)
3217e-8	35	10	6
Rotational stiffness of fastening k_{rx} (N·m/rad)	Rotational stiffness of fastening k_{ry} (N·m/rad)	Rotational stiffness of fastening k_{rz} (N·m/rad)	Fastening spacing l (m)
3.5e5	5e6	7e4	0.635

where $\mathbf{D}$ is the dynamic stiffness matrix. Subscripts L and R refer to the left and right boundary of the unit cell, and I refers to the interior degree of freedoms of the unit cell. For free wave motion, $\mathbf{F}_I = 0$, the condensed equation of motion can be obtained:

$$\begin{bmatrix} \widetilde{\mathbf{D}}_{LL} & \widetilde{\mathbf{D}}_{LR} \\ \widetilde{\mathbf{D}}_{RL} & \widetilde{\mathbf{D}}_{RR} \end{bmatrix} \begin{Bmatrix} \mathbf{U}_L \\ \mathbf{U}_R \end{Bmatrix} = \begin{Bmatrix} \mathbf{F}_L \\ \mathbf{F}_R \end{Bmatrix} \tag{3}$$

According to the Bloch theory [22], the displacements and forces at one cell are related to those of the next cell by Bloch wavenumber κ as follows:

$$\begin{aligned} \mathbf{U}_R &= e^{i\kappa l}\mathbf{U}_L, \\ \mathbf{F}_R &= -e^{i\kappa l}\mathbf{F}_L \end{aligned} \tag{4}$$

where l represents the length of the unit cell.

Combining (3) and (4), the quadratic eigenvalue problem is formulated:

$$\left[\widetilde{\mathbf{D}}_{LR}e^{2i\kappa l} + \left(\widetilde{\mathbf{D}}_{LL} + \widetilde{\mathbf{D}}_{RR}\right)e^{i\kappa l} + \widetilde{\mathbf{D}}_{RL}\right]\{\mathbf{U}_L\} = 0 \tag{5}$$

Equation (5) can be reduced to the linear eigenvalue equation as follows:

$$\left(\begin{bmatrix} \widetilde{\mathbf{D}}_{RL} & \widetilde{\mathbf{D}}_{RR} \\ 0 & \mathbf{I} \end{bmatrix} - e^{i\kappa l}\begin{bmatrix} -\widetilde{\mathbf{D}}_{LL} & -\widetilde{\mathbf{D}}_{LR} \\ \mathbf{I} & 0 \end{bmatrix}\right)\begin{Bmatrix} \mathbf{U}_L \\ \mathbf{U}_R \end{Bmatrix} = 0 \tag{6}$$

By solving the eigenvalue equation in the reduced Brillouin zone $[0, \pi/l]$, the dispersion curves and wave modes of infinite periodic track structure can be obtained.

To analyze the sensitivities of the wave modes to rail axial force more precisely, a wave finite element model of the ballastless track structure is established. The parameters of the tracks structure are listed in Table 1. The rail is simulated with solid elements and the cross section of rail is considered. Since the vibration of rail is close related to the constraint conditions, a detailed fastening model consisted of rail pad, base plate, elastic pad, and fastener clamping force is considered, as shown in Figure 2.

Figure 3 shows the dispersion curves of the periodic track structure base on the wave finite element method, and the corresponding wave modes are shown in Table 2. It is worth

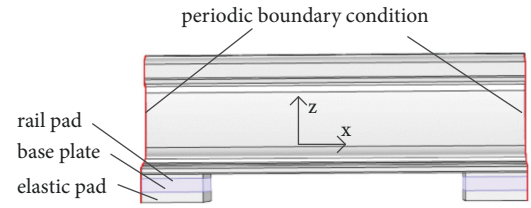

Figure 2: Unit cell [10].

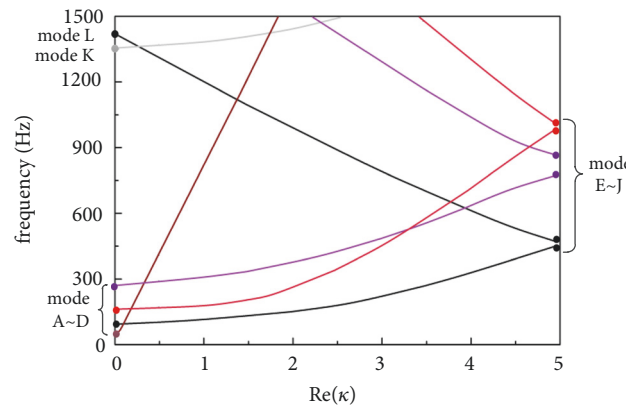

Figure 3: Dispersion curves (red: vertical flexural wave; black: lateral flexural wave; purple: lateral bending-torsion coupling wave; brown: longitudinal wave; gray: torsional wave).

mentioning that the lateral flexural wave is coupled with the torsion wave. The black dispersion curve in Figure 3 is dominated by bending motion, such as mode E and mode F. At $k = 0$, the standing wave modes (mode A ~ mode D) are rigid modes of the rail below 400Hz, which are less affected by the axial force. Above 400Hz, the wave modes are related to the axial force due to the rail bending. Below 1500Hz and at $k = \pi/l$, there are 6 standing wave modes, which are expressed as mode E ~ mode J. Mode E and mode I are 1st order lateral and vertical pinned-pinned modes, respectively. Mode G is similar to mode E, while the bending deformation of mode G is significant at the rail bottom, and the rail head and bottom are subject to antiphase motion. Except mode K, mode E ~ mode L belong to the bending motions, and these bending wave modes might be helpful for the rail axial force estimation.

Table 2: Wave modes of infinite periodic ballastless track structure [10].

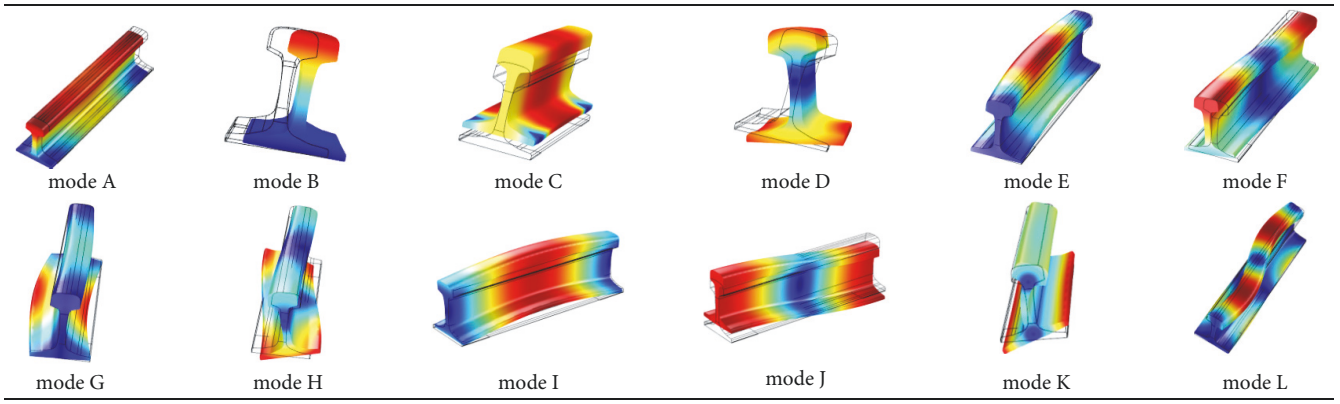

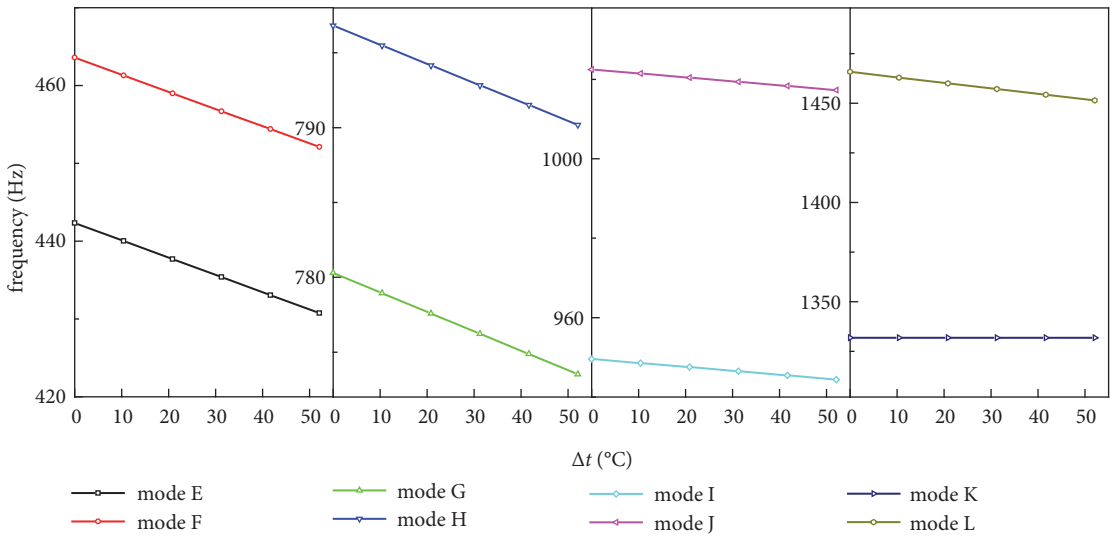

Figure 4: Sensitivities of wave modes to the rail axial force.

Figure 4 shows the sensitivities of different wave modes to the rail axial force. As shown in the figure, mode E~ mode H vary with the rail axial force in linear manner approximately. The sensitivity of both mode E and mode F is 0.22Hz/°C, while the sensitivity mode G and mode H is 0.13Hz/°C. Mode I and mode J are linear with rail axial force with a rate of 0.10Hz/°C, while mode K is not affected by the rail axial force. Mode L is also approximately linear to the rail axial force with the rate of 0.28Hz/°C.

According to the results shown in Figure 4, wave mode I and mode J change with the rail axial force linearly; however, the sensitivity is low. The mode E and mode F are more sensitive to the rail axial force, and these wave modes can be easily excited and measured. In order to make a further selection of the rail axial force indices for ballastless track, an in situ experimental research is conducted.

3. In Situ Experiment

In order to verify the correctness and feasibility of the theoretical analysis, an in situ experiment is conducted in the ballastless track, as shown in Figure 5. Modal test method is adopted to measure the wave modes. The responses of the rail are collected with accelerometers, and the temperature of the rail is monitored by the noncontact thermometers.

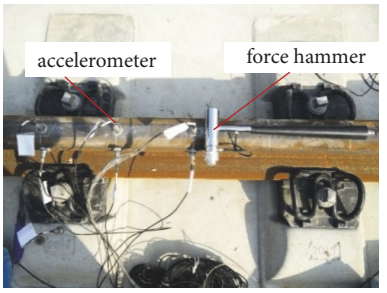

Figure 5: In situ experiment.

3.1. Vertical Wave Mode. When the rail is excited vertically at the mid-span, the receptance functions under different temperatures can be obtained; see Figure 6. According to the frequency response functions, mode C and mode I

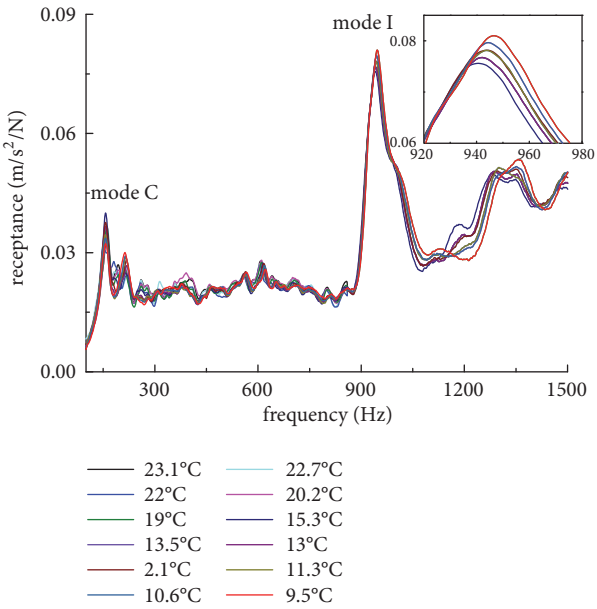

Figure 6: Receptance functions of the rail under different temperatures.

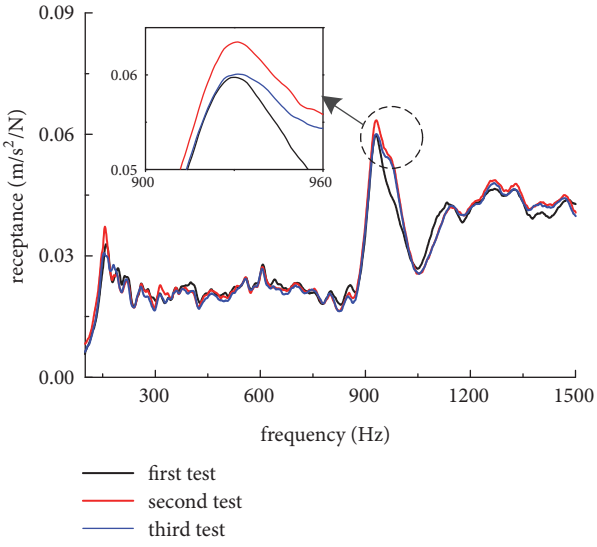

Figure 7: Results of repeated tests.

can be excited significantly. Along with the decrease of the temperature, the vertical 1st order pinned-pinned frequency increases.

However, there might be instabilities and randomness for the force hammer excitation. It is difficult to obtain completely consistent results in the repeated tests due to different hammering forces and positions; see Figure 7. Hence, obvious errors might be caused if the rail axial force is evaluated according to the receptance functions.

Therefore, a multipoint excitation-multipoint pickup modal test is used to obtain more accurate results; see Figure 8. The wave modes and frequencies of the rail are measured simultaneously under different temperatures.

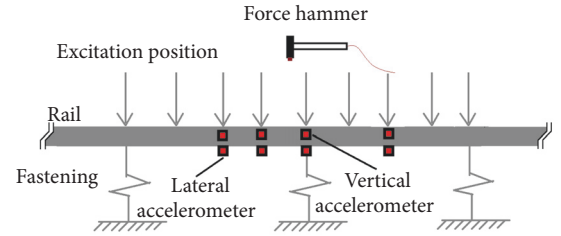

Figure 8: Modal test.

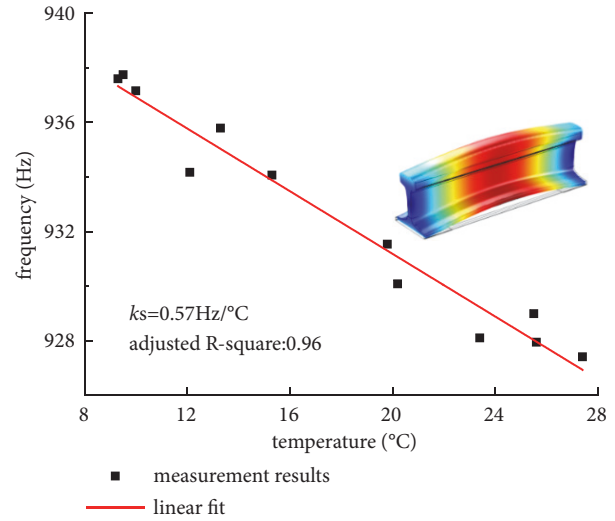

Figure 9: Relation of vertical 1st order pinned-pinned wave mode to the rail temperature.

The vertical pinned-pinned frequencies (wave mode I) under different temperatures are obtained through modal test; see Figure 9. The measured sensitivity of mode I to the temperature is 0.57Hz/°C, which is quite different from the theoretical one. Therefore, a further analysis is required. Since the vertical wave mode might be affected by constraint conditions, the parametric analysis of the fastening system will be discussed in detail in Section 4.

3.2. Lateral Wave Mode. Figure 10 shows the receptance function when the mid-span of rail is excited laterally, and most of the lateral standing wave modes below 1500Hz can be excited effectively.

Similarly, the lateral standing wave modes and frequencies of the rail under different temperatures are obtained. The sensitivity of mode E (first order lateral pinned-pinned wave mode) to the rail temperature is shown in Figure 11. In the range of 18°C ~ 35°C, the sensitivity of the wave mode is 0.21Hz/°C, which basically coincided with the theoretical result (0.22Hz/°C). Existing studies have shown that the stiffness of fastening changes nonlinearly with temperature and it is more obvious at low temperatures [23]. In order to validate the stability of the index, repeated in situ tests are carried out. As shown in Figure 12, the sensitivity is also 0.21Hz/°C at lower temperatures (9°C ~ 28°C), indicating

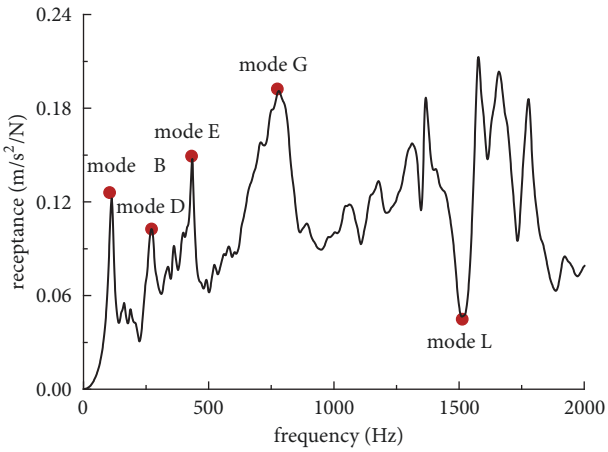

FIGURE 10: Lateral vibration receptance function at mid-span of rail.

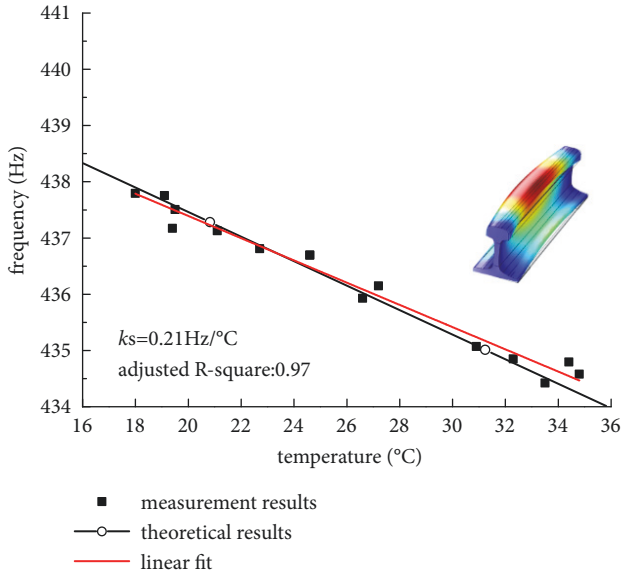

FIGURE 11: Relation of lateral 1st order pinned-pinned wave mode to the rail temperature.

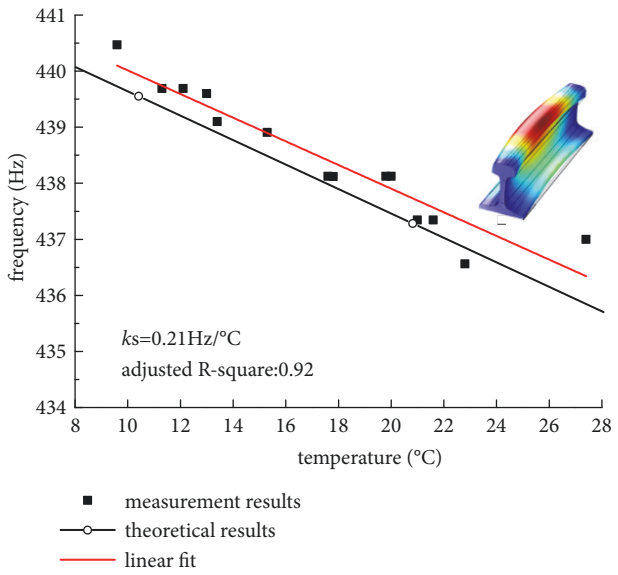

FIGURE 12: The lateral 1st order pinned-pinned wave mode performance at lower temperatures.

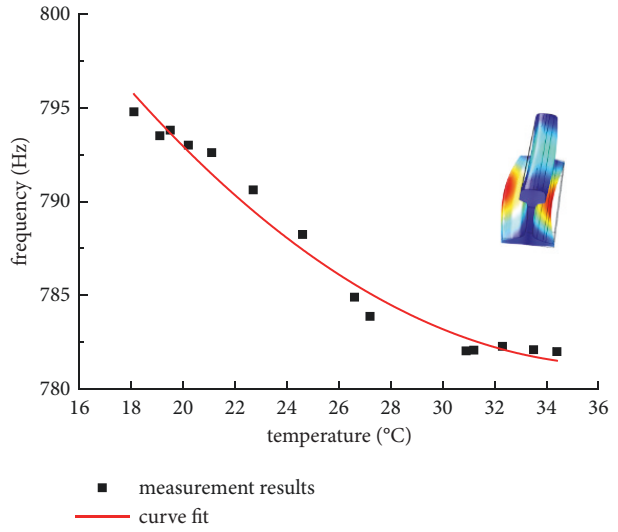

FIGURE 13: Variation of mode G with rail temperature.

that the index is reliable for measuring the rail axial force in ballastless track.

Furthermore, the theoretical results are also plotted in the figures. There is a good agreement with the measurement results of the first test, while a small difference (about 0.5Hz) appears in the repeated test. This might be caused by the installation positions of the sensors. Besides, the discreteness of the measurement results is small, and the maximum error is 0.7Hz, corresponding to 3.5°C. This error can be further reduced by multiple tests.

Figure 13 shows the sensitivity of mode G to the rail temperature, and the change of the frequency with the temperature is nonlinear. According to the existing research findings [24, 25], the stiffness of elastic pad increases nonlinearly with the decrease of the temperature. Meanwhile, the deformation of wave mode G occurs mainly at the rail foot, which will be greatly affected by the temperature-dependent characteristic of the fastening. Therefore, this wave mode is not suitable for rail axial force estimation.

The sensitivity of lateral 2nd order pinned-pinned wave mode (mode L) is 0.65Hz/°C as shown in Figure 14, while the theoretical result is 0.28Hz/°C. For high frequency vibrations, it is hard to obtain accurate results through the force hammer excitation. So, there is a high discreteness of the test results under different temperatures.

4. Influence Factors

The sensitivities of wave modes in high-speed railway ballastless track structure under different temperatures were tested by the in situ experiment. It can be concluded that the lateral 1st order pinned-pinned wave mode is coincided with the

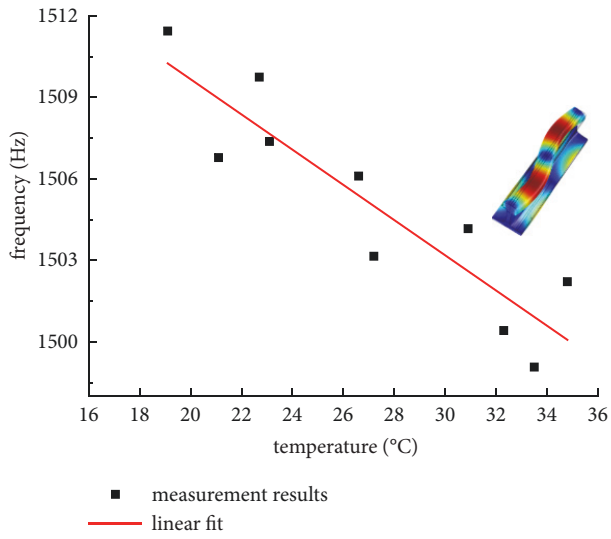

FIGURE 14: Relation of lateral 2nd pinned-pinned wave mode to the rail temperature.

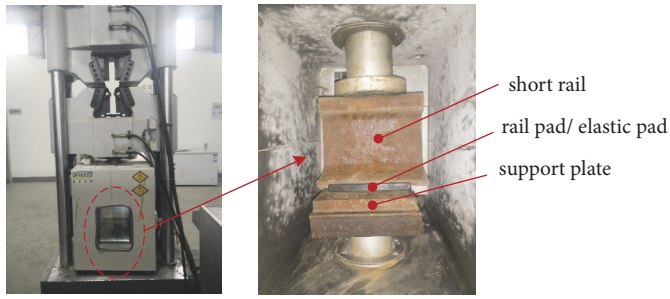

FIGURE 15: Temperature-dependent experiment.

theoretical result, while the vertical 1st order pinned-pinned wave mode is quite different from the theoretical result. Since the wave modes of the rail can be affected by the fastening system in ballastless track structure. In order to explicate the in situ experiment results, influences of fastening parameters on the rail axial force estimation are discussed according to the temperature-dependent experiment in this section.

4.1. Temperature-Dependent Experiment. Many research findings show that the fastening system parameters are closely related to the temperature [23–26]. The temperature-dependent experiment is conducted for rail pad and elastic pad of the ballastless track. The universal testing machine is equipped with a temperature control box; see Figure 15. A force transducer measures the force transmitted to the sample while the deformation of the sample is measured using a displacement sensor. Since the fastening is mainly consisted of rail pad, base plate, and elastic pad, and the stiffness of the fastening is basically provided by the rail pad and elastic pad, the temperature-dependent properties of rail pad and elastic pad should be studied. The stiffness of the rail pad and elastic pad is measured at -10°C ~ 40°C; then, the modulus can be calculated according to the method in reference [25]. As shown in Figure 16, both the elastic modulus of the rail pad and elastic pad increase with the decrease of the temperature, while the rail pad is more sensitive to the temperature.

4.2. Parametric Analysis. Influences of the temperature-dependent parameters (rail pad stiffness, elastic pad stiffness, and fastener clamping force) of the fastening system on the rail axial force estimation are analyzed in this section. Figure 17 shows the influence of rail pad temperature-dependent property on vertical 1st order pinned-pinned wave mode. According to the test result in Figure 16, when temperature decreases from 40°C to 10°C (corresponding to the in situ experiment in Section 3), the modulus of the rail pad will increase from 80Mpa to 90Mpa approximately. Based on the wave finite element model, only considering the effects of temperature-dependent parameters, the vertical 1st order pinned-pinned wave mode will increase from 945Hz to 953Hz. In addition, the vertical pinned-pinned wave mode will also increase with the increase of the elastic pad stiffness. Therefore, the frequency shift of the vertical 1st order pinned-pinned wave mode with the temperature measured in the in situ experiment is mainly caused by the temperature-dependent characteristics of the rail pad and elastic pad.

In addition, the clamping force of the fastener is an important part of the fastening system. Because the clamping forces are mainly provided by the pretightening of spiral nail,

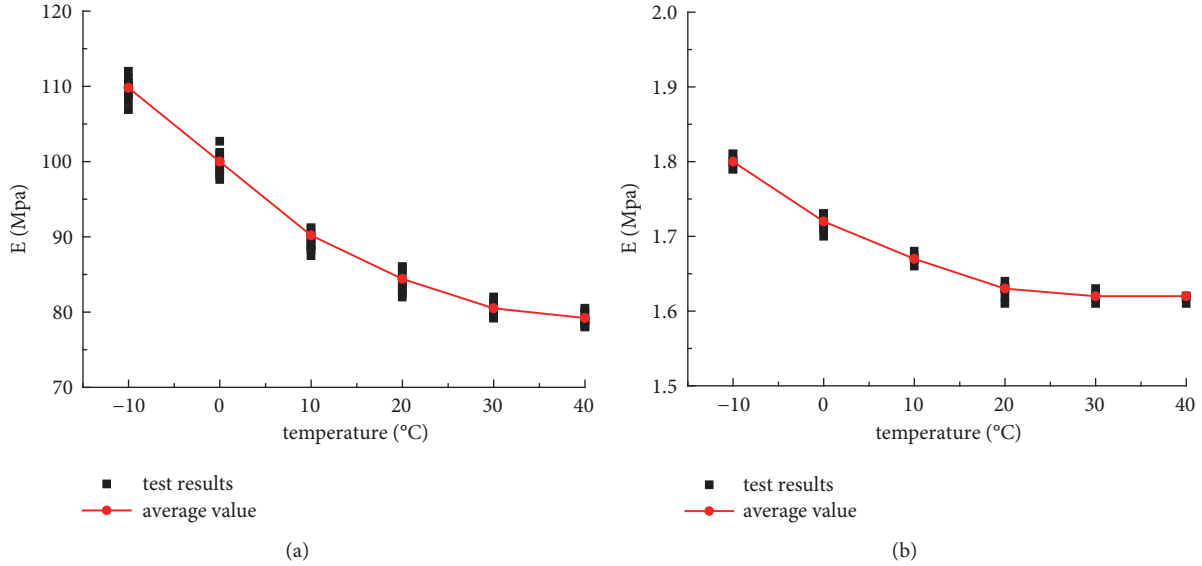

Figure 16: Temperature-dependent rail pad/elastic pad. (a) Rail pad and (b) elastic pad.

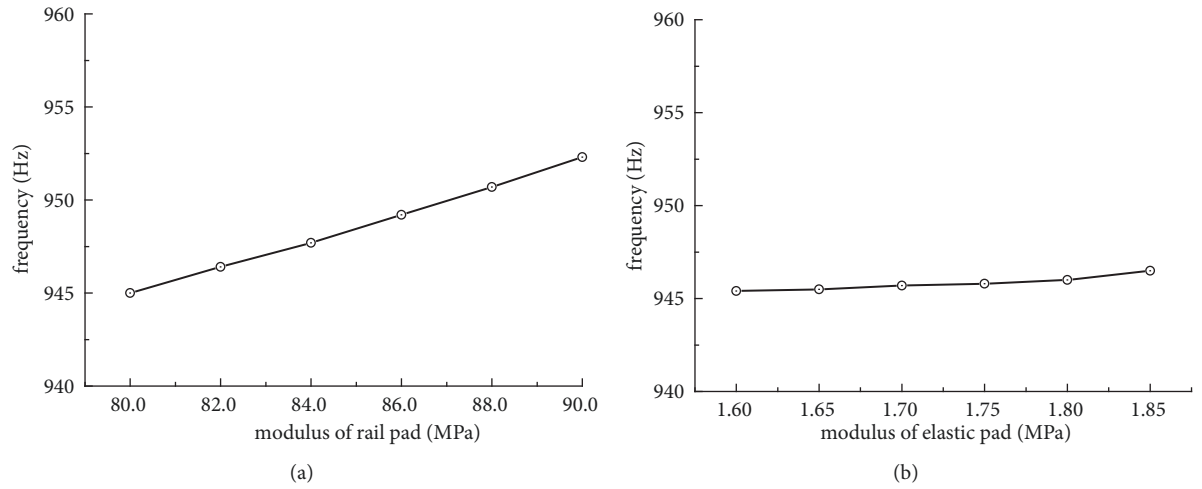

Figure 17: Influences of modulus of rail pad/elastic pad on the vertical 1st order pinned-pinned wave mode. (a) Rail pad; (b) elastic pad.

it might be changed with the temperature. It is regrettable that the clamping force of the fastener is not tested because of the limited test condition, so only a theoretical analysis based on the wave finite element model is presented here. Theoretical results show that the vertical pinned-pined wave mode will increase from 946Hz to 952Hz, when the clamping force of the fastener decreases from 10kN to 2kN; see Figure 18.

According to the above analysis, the vertical pinned-pinned wave mode is closely related to the temperature-dependent properties of the fastening system. The frequency shift with different temperatures is mainly caused by the temperature-dependent parameters of the fastening system. Hence, the law of the vertical pinned-pinned wave mode measured in Section 3 is quite different from the theoretical one.

Meanwhile, for the lateral 1st order pinned-pinned wave mode, the influences of the fastening temperature- dependent parameters are discussed, as shown in Figures 19 and 20.

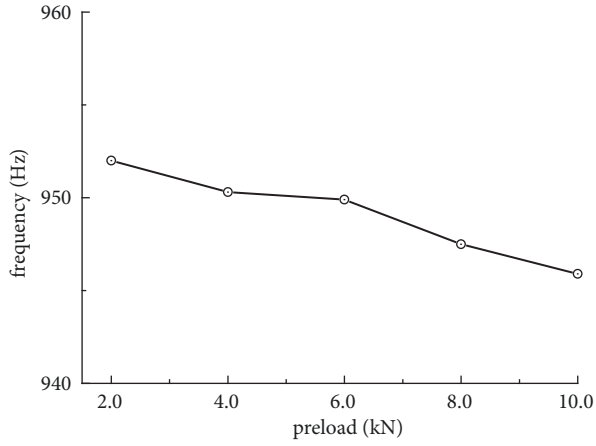

Figure 18: Influences of fastener clamping force on the vertical 1st order pinned-pinned wave mode.

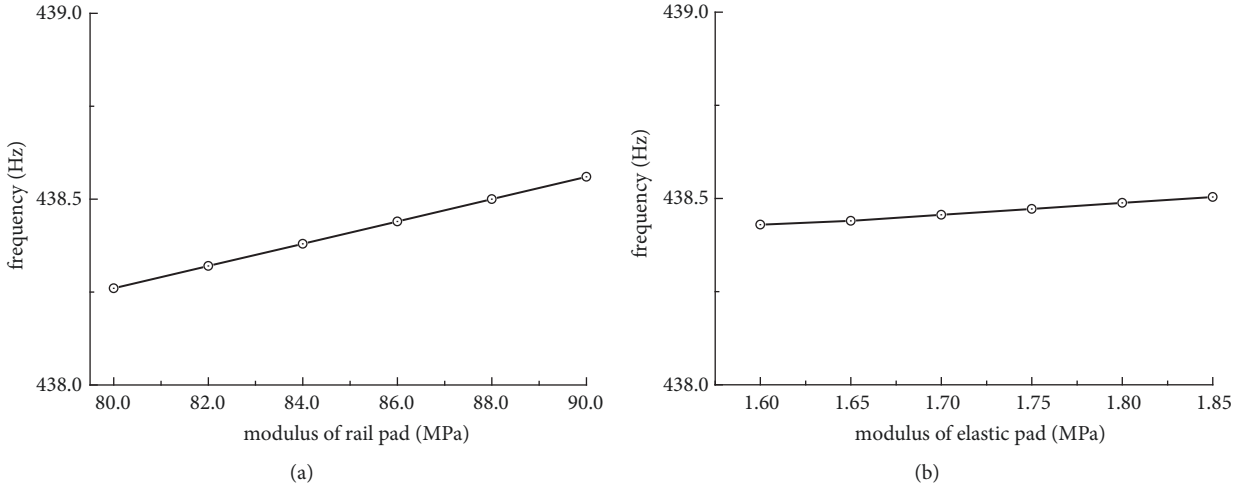

Figure 19: Influences of modulus of rail pad/elastic pad on the lateral 1st order pinned-pinned wave mode. (a) Rail pad; (b) elastic pad.

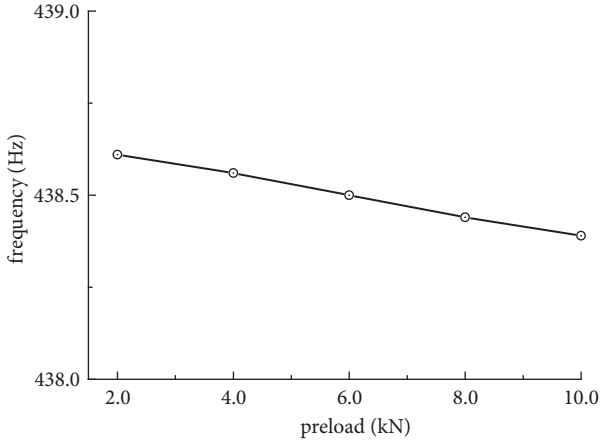

Figure 20: Influences of fastener clamping force on the lateral 1st order pinned-pinned wave mode.

The lateral pinned-pinned frequency increases with the increase of the rail pad/elastic pad modulus; however, the variation is extremely small. For the rail pad, when the modulus increases from 80Mpa to 90Mpa, the lateral pinned-pinned frequency only increases by 0.3Hz; for the elastic pad, when modulus increases from 1.6Mpa to 1.85Mpa, the lateral pinned-pinned frequency only increases by 0.15Hz. Similarly, the fastener clamping force also has little effect on the lateral pinned-pinned wave mode.

In summary, fastening temperature-dependent parameters can affect the vertical pinned-pinned wave mode obviously; however, frequency shift of the lateral 1st order pinned-pinned wave mode is mainly determined by the rail axial force. Therefore, the lateral 1st order pinned-pinned wave mode can be used for estimating the rail axial force in ballastless track directly and do not need any error correction process.

In order to apply this method in practice, the modal test instead of frequency response function is adopted and this method is easy to estimate the relative rail axial force. Although only the relative rail axial force is discussed in the present study, this method can be extended to the absolute rail axial force measurement. To measure the absolute rail axial force, exact parameters of the track structure need to be determined, especially the dynamic parameters of fastening. The dynamic parameters of fastening can be determined experimentally [25]. Therefore, the absolute axial force estimation according to the wave modes should be studied in the future research.

5. Conclusion

For the ballastless track in high-speed railway, the elasticity is mainly provided by the fastening and the track structure has obvious periodic characteristics due to the high requirements of design and construction. Therefore, it is feasible to measure the rail axial force based on the wave mode without complex measuring or any error correction process. This paper studied the rail axial force estimation in high-speed railway ballastless track theoretically and experimentally. The following conclusions can be drawn.

(1) The flexural wave modes of ballastless track are sensitive to the rail axial force. Theoretical results show that the sensitivity of the vertical 1st order pinned-pinned wave mode is 0.10Hz/°C, while the lateral 1st order pinned-pinned wave mode is 0.22Hz/°C.

(2) The in situ experiment results show that the lateral pinned-pinned wave mode coincides well with the theoretical result, while there is a large difference for the vertical pinned-pinned wave mode.

(3) According to the temperature-dependent experiment of the fastening system, when the temperature decreases from 40°C to 10°C, the stiffness of the rail pad increases obviously; however, the variation of elastic pad is minor. Combining with the parametric analysis, the temperature-dependent parameters can greatly affect the vertical pinned-pinned wave mode, while they have little influence on the lateral pinned-pinned wave mode, and the different behaviors

of the wave modes in the in situ experiment can be explicated consequently. Therefore, it is suggested that the 1st order lateral pinned-pinned wave mode can be adopted as the index for estimating the rail axial force.

Data Availability

The data used to support the findings of this study are included within the article.

Conflicts of Interest

The authors declare that they have no conflicts of interest.

Acknowledgments

Thanks are due to the National Key Research and Development Program of China (2016YFE0205200) and NSFC (National Natural Science Foundation of China, No. 51425804) for the research grant awarded to this paper. The work described in this paper is supported by the National Natural Science Foundation of China (51508479), the Doctoral Innovation Fund Program of Southwest Jiaotong University, and the Research Fund for Key Research and Development Projects in Sichuan Province (2017GZ0373).

References

[1] V. Srinivas, K. Ramanjaneyulu, K. Saravana Kumar et al., "Evaluation of Longitudinal Force on a Railway Bridge Based on Strain Measurements," *Experimental Techniques*, vol. 37, no. 1, pp. 55–67, 2013.

[2] Y. Zhao, Y. Zhao, and M. Zhao, "Novel force sensor based on a couple of fiber bragg gratings," *Measurement*, vol. 38, no. 1, pp. 30–33, 2005.

[3] P. Wang, K. Xie, L. Shao, L. Yan, J. Xu, and R. Chen, "Longitudinal force measurement in continuous welded rail with bidirectional FBG strain sensors," *Smart Materials and Structures*, vol. 25, no. 1, Article ID 015019, 2016.

[4] Y. Wen, S. Liu, Y. Zhang et al., "A rail vibration test and analysis method for the electromagnetic launching process [J]," *Measurement*, vol. 85, pp. 232–238, 2016.

[5] D. Vangi and A. Virga, "A Practical Application of Ultrasonic Thermal Stress Monitoring in Continuous Welded Rails," *Experimental Mechanics*, vol. 47, no. 5, pp. 617–623, 2007.

[6] T. Sasaki, S. Takahashi, Y. Kanematsu et al., "Measurement of residual stresses in rails by neutron diffraction," *Wear*, vol. 265, no. 9-10, pp. 1402–1407, 2008.

[7] W. Koc and A. Wilk, "Investigations of methods to measure longitudinal forces in continuous welded rail tracks using the tamping machine," *Proceedings of the Institution of Mechanical Engineers, Part F: Journal of Rail and Rapid Transit*, vol. 223, no. 1, pp. 61–73, 2009.

[8] Y. Sato, "Study on measurement of rail longitudinal force on slab track by rail lifting[J]," *WIT Transactions on the Built Environment*, vol. 61, no. 1, pp. 571–580, 2002.

[9] R. L. Weaver, "Vibration measurement of rail stress," *High-Speed Rail IDEA Program Project Final Repor t[R]*, 2006.

[10] P. Wang, Q. Yi, C. Zhao, and M. Xing, "Elastic wave propagation characteristics of periodic track structure in high-speed railway," *Journal of Vibration and Control*, vol. 25, no. 3, pp. 517–528, 2018.

[11] Y. Luo, "A model for predicting the effect of temperature force of continuous welded rail track," *Proceedings of the Institution of Mechanical Engineers, Part F: Journal of Rail and Rapid Transit*, vol. 213, no. 2, pp. 117–124, 1999.

[12] Y. Luo, L. Li, and H. Yin, "A dynamic analysis of a continuous welded rail track under a longitudinal stress caused by temperature changes," *Proceedings of the Institution of Mechanical Engineers, Part F: Journal of Rail and Rapid Transit*, vol. 224, no. 2, pp. 91–101, 2010.

[13] V. Damljanović and R. L. Weaver, "Laser vibrometry technique for measurement of contained stress in railroad rail," *Journal of Sound and Vibration*, vol. 282, no. 1-2, pp. 341–366, 2005.

[14] G. Kjell and E. Johnson, "Measuring axial forces in rail by forced vibrations: experiences from a full-scale laboratory experiment," *Proceedings of the Institution of Mechanical Engineers, Part F: Journal of Rail and Rapid Transit*, vol. 223, no. 3, pp. 241–254, 2009.

[15] Y. Guo, Z. Yu, and H. Shi, "Effects of rail thermal stress on the dynamic response of vehicle and track," *Vehicle System Dynamics*, vol. 53, no. 1, pp. 30–50, 2014.

[16] A. Aikawa, H. Sakai, and K. Abe, "Numerical and experimental study on measuring method of rail axial stress of continuous welded rails based on use of resonant frequency," *Quarterly Report of RTRI*, vol. 54, no. 2, pp. 118–125, 2013.

[17] F. Urakawa, K. Abe, and H. Takahashi, "Improvement of accuracy of method for measuring axial force of rail based on natural frequency," *Quarterly Report of RTRI (Railway Technical Research Institute)*, vol. 57, no. 2, pp. 125–132, 2016.

[18] P. Wang, Q. Yi, C. Zhao, M. Xing, and J. Tang, "Wave propagation in periodic track structures: band-gap behaviours and formation mechanisms," *Archive of Applied Mechanics*, vol. 87, no. 3, pp. 503–519, 2017.

[19] F. Dai, D. J. Thompson, Y. Zhu, and X. Liu, "Vibration properties of slab track installed on a viaduct," *Proceedings of the Institution of Mechanical Engineers, Part F: Journal of Rail and Rapid Transit*, vol. 230, no. 1, pp. 235–252, 2014.

[20] B. An, D. Ma, P. Wang et al., "Assessing the fast non-Hertzian methods based on the simulation of wheel–rail rolling contact and wear distribution," *Proceedings of the Institution of Mechanical Engineers, Part F: Journal of Rail and Rapid Transit*, p. 095440971984859, 2019.

[21] P. Wang, X. Ma, J. Xu, J. Wang, and R. Chen, "Numerical investigation on effect of the relative motion of stock/switch rails on the load transfer distribution along the switch panel in high-speed railway turnout," *Vehicle System Dynamics*, vol. 57, no. 2, pp. 226–246, 2019.

[22] D. J. Mead, "The forced vibration of one-dimensional multi-coupled periodic structures: an application to finite element analysis," *Journal of Sound and Vibration*, vol. 319, no. 1, pp. 282–304, 2009.

[23] M. Oregui, A. d. Man, M. Woldekidan, Z. Li, and R. Dollevoet, "Obtaining railpad properties via dynamic mechanical analysis," *Journal of Sound and Vibration*, vol. 363, pp. 460–472, 2016.

[24] N. Ahmad, "A methodology for developing high damping materials with application to noise reduction of railway track," *The Journal of the Acoustical Society of America*, vol. 126, no. 6, p. 3373, 2009.

[25] G. Squicciarini, D. J. Thompson, M. G. Toward, and R. A. Cottrell, "The effect of temperature on railway rolling noise," *Proceedings of the Institution of Mechanical Engineers, Part F: Journal of Rail and Rapid Transit*, vol. 230, no. 8, pp. 1777–1789, 2016.

[26] M. Oregui, A. Núñez, R. Dollevoet, and Z. Li, "Sensitivity analysis of railpad parameters on vertical railway track dynamics," *Journal of Engineering Mechanics*, vol. 143, no. 5, 2017.